Macroscopic traffic flow modelling: from kinematic waves to autonomous vehicles

Paola Goatin

sciendo

CAIM
ISSN 2038-0909

Commun. Appl. Ind. Math. 13 (1), 2022, 1–16 DOI: 10.2478/caim-2022-XXXX

Review Article

Macroscopic traffic flow modelling: from kinematic waves to autonomous vehicles

Paola Goatin[1*]

[1]Université Côte d'Azur, Inria, CNRS, LJAD, Sophia Antipolis, France.

[*]Email address for correspondence: paola.goatin@inria.fr

Communicated by Associate Editor

Received on XXXX XX, XXXX. Accepted on XXXX XX, XXXX.

Abstract

This survey offers a unified up-to-date presentation of macroscopic models of traffic flow, pointing out their main characteristics and possible drawbacks. The presentation is completed by several pictures illustrating the models' features. Some open problems and future research directions are also given to inspire the reader.

Keywords: `Macroscopic traffic models; hyperbolic systems of conservation laws; finite volume schemes; PDE-ODE systems.`

AMS subject classification: `35L65, 90B20, 82B21`

1. Introduction

Macroscopic traffic flow models consist of partial differential equations derived from fluid dynamics to describe the spatio-temporal evolution of locally aggregated quantities such as the traffic density ρ and the mean velocity v. Starting from the fundamental assumption that the number of cars on a road segment is conserved, one easily recovers a mass conservation law in one space dimension, in the form

$$\partial_t \rho + \partial_x q = 0, \qquad x \in \mathbb{R},\ t > 0, \tag{1}$$

where $\rho = \rho(t,x) \geq 0$ is number of vehicles per space unit and $q = q(t,x) \geq 0$ is the flow, expressed as number of vehicles per time unit. The fundamental hydrodynamic relation $q = \rho v$ allows to rewrite (1) as

$$\partial_t \rho + \partial_x (\rho v) = 0, \qquad x \in \mathbb{R},\ t > 0, \tag{2}$$

where we assume homogeneous road conditions with $\rho = \rho(t,x) \in [0, R_{\max}]$ and $v = v(t,x) \in [0, V_{\max}]$, $R_{\max}$ and $V_{\max}$ denoting respectively the maximal density and the maximal speed that can be attained on the considered road.

To close equation (2), one needs to add information on the speed function v. In the mid 1950's, Lighthill, Whitham [1] and Richard [2] proposed a functional dependence on the density, assuming $v = v_e(\rho)$, thus providing the *first order* LWR model

$$\partial_t \rho + \partial_x (\rho v_e(\rho)) = 0, \qquad x \in \mathbb{R},\ t > 0, \tag{3}$$

according to which the traffic density ρ solves a scalar conservation law. The function $v_e : [0, R_{\max}] \to [0, V_{\max}]$ is commonly assumed to be non-increasing, with $v_e(0) = V_{\max}$ and $v_e(R_{\max}) = 0$, modeling the fact that, when the road is empty, drivers can run at the maximal allowed speed, while they have to stop at maximal (bumper-to-bumper) traffic density. Of course, different choices of the speed function lead to different flux functions, see for example Figure 1, but $q_e(\rho) = \rho v_e(\rho)$ is usually required to have a unique point of maximum ρ_{cr}, referred to as the *critical density*, so that q_e is increasing on $[0, \rho_{cr}[$ and decreasing on $]\rho_{cr}, R_{\max}]$: $q_e'(\rho)(\rho_{cr} - \rho) \geq 0$ for $\rho \in [0, R_{\max}]$.

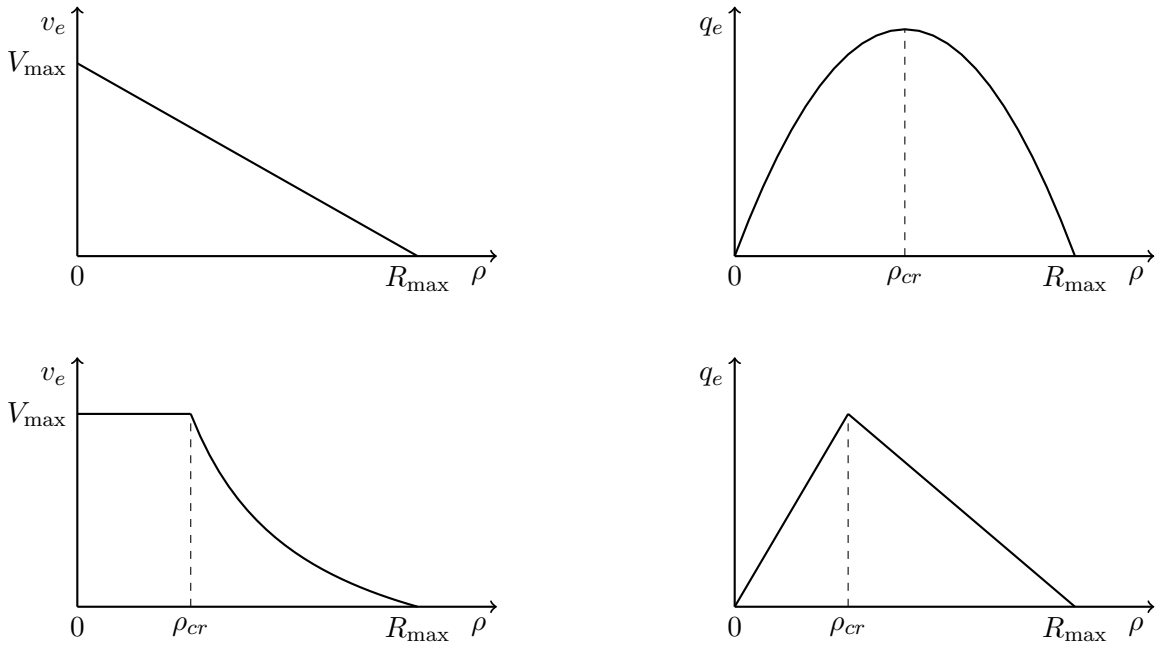

Figure 1. Speed-density (left) and flow-density (right) fundamental diagrams corresponding to two common choices of the speed function. Top: $v_e(\rho) = V_{\max}\left(1 - \frac{\rho}{R_{\max}}\right)$ (Greenshields' fundamental diagram). Bottom: $v_e(\rho) = \min\left\{V_{\max}, w\left(\frac{R_{\max}}{\rho} - 1\right)\right\}$ (triangular fundamental diagram).

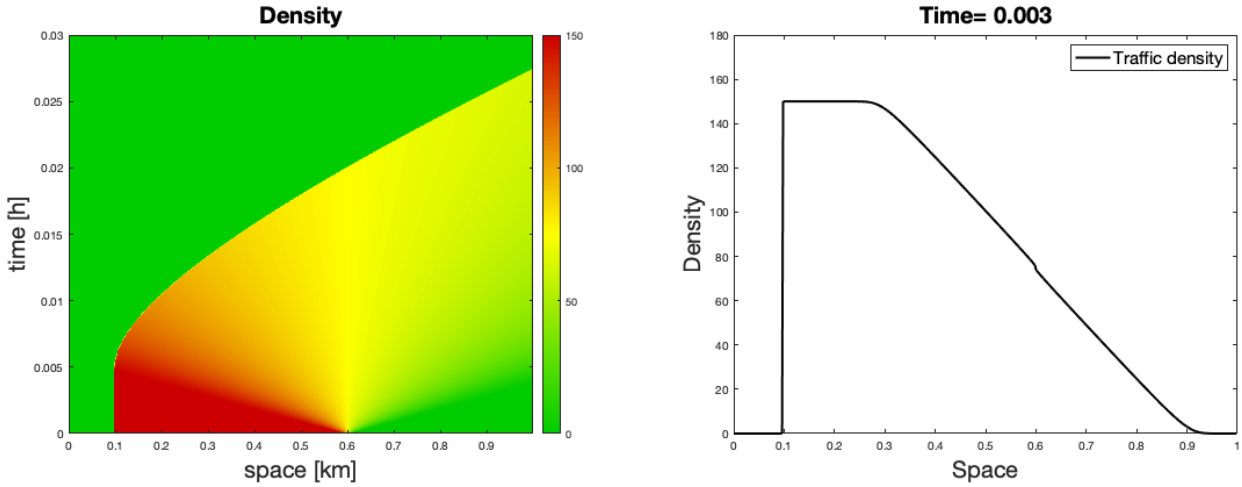

Figure 2. Solution of (3) with $v_e(\rho) = V_{\max}\left(1 - \frac{\rho}{R_{\max}}\right)$, where $V_{\max} = 100$ km/h and $R_{\max} = 150$ veh/km, corresponding to the initial datum $\rho^0(x) = R_{\max}\chi([0.1, 0.6])$ and describing queue dissolution at a traffic light located at $x = 0.6$ and turning to green at $t = 0$. Left: (t, x) plot. Right: density profile at $t = 0.003$ h. We can observe the upstream shock and the downstream rarefaction, which start interacting after $t = 0.005$ h.

LWR model (3) allows to capture some basic features of traffic on road networks, such as congestion formation and propagation and queue dissolution, see Figure 2 for an example of solution to (3) consisting of an upstream shock interacting with a downstream rarefaction wave. Nevertheless, the assumed functional dependency of the average velocity on the traffic density, which holds at equilibrium, can be far from real behaviour in some situations. Indeed, it assumes that drivers can adjust instantaneously their velocities according to the densities they are experiencing, thus implying infinite acceleration of the vehicles. To overcome these limitations, *second order models* consist of an additional dynamical acceleration equation for v, thus resulting in 2×2 systems of balance laws, which capture traffic instabilities,

capacity drop phenomena and scattered flow-density data, see e.g. [3,4]. The second order model proposed by Payne [5] and Whitham [6] suffered of some drawbacks, such as the presence of negative velocities under certain circumtances [7]. An alternative model was then proposed by Aw, Rascle [8] and Zhang [9], whose non-conservative formulation reads as

$$\begin{cases} \partial_t \rho + \partial_x(\rho v) = 0, \\ \partial_t v + (v - \rho p'(\rho))\partial_x v = \dfrac{v_e(\rho) - v}{\tau}, \end{cases} \qquad x \in \mathbb{R},\ t > 0, \tag{4}$$

for some function p satisfying $p(\rho) > 0$, $p'(\rho) > 0$ and $2p'(\rho) + \rho p''(\rho) > 0$ for $\rho > 0$. This pseudo-pressure accounts for drivers' anticipation of downstream density changes. The source term expresses the willing of drivers to adapt their speed to the equilibrium one, $\tau \geq 0$ being the relaxation time parameter.
We observe that the conservative form of (4) writes

$$\begin{cases} \partial_t \rho + \partial_x(\rho v) = 0, \\ \partial_t(\rho(v + p(\rho))) + \partial_x(\rho v(v + p(\rho))) = \rho\dfrac{v_e(\rho) - v}{\tau}, \end{cases} \qquad x \in \mathbb{R},\ t > 0, \tag{5}$$

see Figure 3 for the corresponding speed-density and flux-density fundamental diagrams. Figure 4 shows

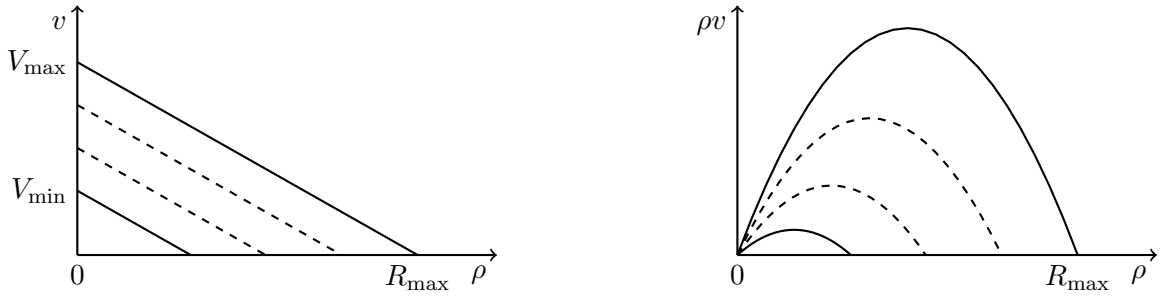

Figure 3. Speed-density (left) and flow-density (right) fundamental diagrams for the ARZ model (5) corresponding to the choice $p(\rho) = w - \alpha\rho$, with $w \in [V_{\min}, V_{\max}]$ and $\alpha > 0$. We observe that the model allows for zero flux (and zero average speed) for densities belonging to the interval $1/\alpha \cdot [V_{\min}, V_{\max}]$, and not for a sigle (maximal) density value. This may model different types of more or less aggressive drivers, jamming at higher or lower densities when traffic is stopped.

a solution corresponding to the homogeneous version of (5), where we have set the right-hand side to zero (letting $\tau \to +\infty$). Here, we model the presence of more aggressive drivers willing to run faster, thus causing a congestion upstream the group of slower cars preceding them and resulting in a more complex dynamics than the one in Figure 2, which cannot be captured by the LWR model (3).

Several extensions of the above mentioned models are possible. First of all, model parameters can be space and/or time dependent, to describe heterogeneous road conditions and variable speed limits. Besides, multi-lane dynamics can be handled by systems of balance laws with suitable lane-changing terms [10–12]. Moreover, macroscopic models can be extended to describe traffic flow on road networks by introducing suitable coupling conditions at junction nodes, see e.g. [13] for an overview. Also, non-local dependencies in the flux function have been proposed recently, aiming at modeling the reaction of drivers to downstream traffic conditions [14,15].
These extensions will not be addressed in the present review and we invite the interested reader to refer to the corresponding literature.

2. Macroscopic traffic flow models

The principal macroscopic traffic models mentioned above can be cast in the following class of 2×2 hyperbolic systems of conservation laws, which is referred to as Generic Second Order traffic flow Models

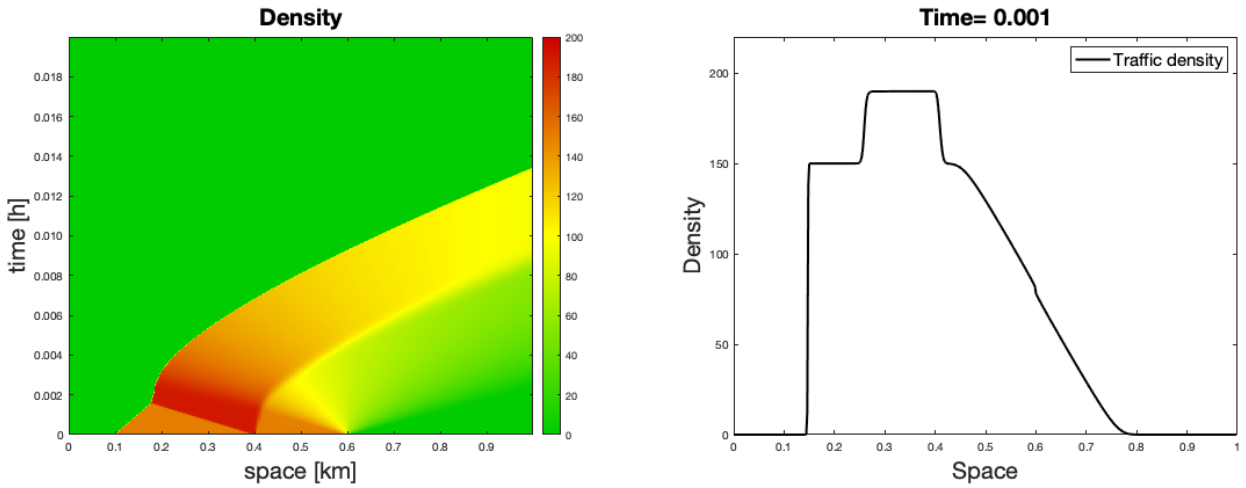

Figure 4. Solution of (5) with $\tau = +\infty$ and $p(\rho) = \rho$, corresponding to the initial datum $\rho^0(x) = 150\chi([0.1, 0.6])$ and $v^0(x) = 50\chi([0.1, 0.4]) + 10\chi(]0.4, 0.6])$. This situation describes queue dissolution at a traffic light located at $x = 0.6$ and turning to green at $t = 0$, with a group of more aggressive divers initially located behind slower ones, which causes a congestion formation behind the downstream group, where density almost reaches value 200. Left: (t, x) plot. Right: density profile at $t = 0.001$ h. We can observe the upstream shock and the downstream rarefaction, separated by an higher density region delimited by an upstream shock and a downstream contact discontinuity separating the two groups of drivers.

(GSOM) [16]:

$$\begin{cases} \partial_t \rho + \partial_x(\rho v) = 0, \\ \partial_t(\rho w) + \partial_x(\rho w v) = 0, \end{cases} \qquad x \in \mathbb{R},\ t > 0, \tag{6}$$

where the average speed of vehicles is a function of the density $\rho = \rho(t, x)$ and a Lagrangian vehicle property $w = w(t, x)$, namely $v = \mathcal{V}(\rho, w)$ for some speed function $\mathcal{V}$ satisfying the following hypotheses [17]:

$$\mathcal{V}(\rho, w) \geq 0, \quad \mathcal{V}(0, w) = w, \tag{7a}$$

$$2\mathcal{V}_\rho(\rho, w) + \rho\mathcal{V}_{\rho\rho}(\rho, w) < 0 \text{ for } w > 0, \tag{7b}$$

$$\mathcal{V}_w(\rho, w) > 0, \tag{7c}$$

$$\forall w > 0 \quad \exists\ R(w) > 0 : \quad \mathcal{V}(R(w), w) = 0. \tag{7d}$$

As in [17,18], we observe that (7b) implies that $Q(\rho, w) := \rho\mathcal{V}(\rho, w)$ is strictly concave and $\mathcal{V}_\rho(\rho, w) < 0$ for $w > 0$, if $\mathcal{V}$ is a $\mathbf{C^2}$ function in ρ. For later use, we denote by $\rho_{cr}(w) \in]0, R(w)[$ the point of maximum of $Q(\rho, w)$ and by $Q_{\max}(w) = Q(\rho_{cr}(w), w)$ the corresponding maximum. We also remark that in (7d) we can have $R(w) = R_{\max}$ for all $w > 0$.

System (6) is strictly hyperbolic for $\rho > 0$, with eigenvalues

$$\lambda_1(\rho, w) = \mathcal{V}(\rho, w) + \rho\mathcal{V}_\rho(\rho, w), \qquad \lambda_2(\rho, w) = \mathcal{V}(\rho, w), \tag{8}$$

and corresponding eigenvectors

$$r_1(\rho, w) = \begin{pmatrix} -1 \\ 0 \end{pmatrix}, \qquad r_2(\rho, w) = \begin{pmatrix} \mathcal{V}_w(\rho, w) \\ -\mathcal{V}_\rho(\rho, w) \end{pmatrix}, \tag{9}$$

with the first characteristic field being genuinely non-linear and the second linearly degenerate [19, Definition 5.2]. The associated Riemann invariants are

$$z_1(\rho, w) = \mathcal{V}(\rho, w), \qquad z_2(\rho, w) = w.$$

Since shock and rarefaction curves of each family coincide, the system belongs to the Temple class [20]. Notice that, setting $\mathcal{V}(\rho, w) = w - p(\rho)$ for a suitable "pressure" function p, system (6) corresponds to the Aw-Rascle-Zhang (ARZ) model (5). We also remark that, taking $w = \bar{w}$ constant, we recover the classical Lighthill-Whitham-Richards (LWR) model (3) with $v_e(\rho) = \mathcal{V}(\rho, \bar{w})$.

We consider for (6) an invariant domain of the form

$$\Omega := \left\{(\rho, w) \in \mathbb{R}^2 \colon \rho \in [0, R(w_{max})], w \in [w_{min}, w_{max}]\right\} \tag{10}$$

for some $0 < w_{min} \leq w_{max} < +\infty$. Since $\mathcal{V}_\rho(\rho, w) < 0$ and $\mathcal{V}(0, w) = w$, the range of $v = \mathcal{V}(\rho, w)$ is given by $v \in [0, w]$ for any $w \in [w_{min}, w_{max}]$. In particular, we have $v = w$ in the vacuum. See Figure 5 for a representation of Ω in different coordinates.

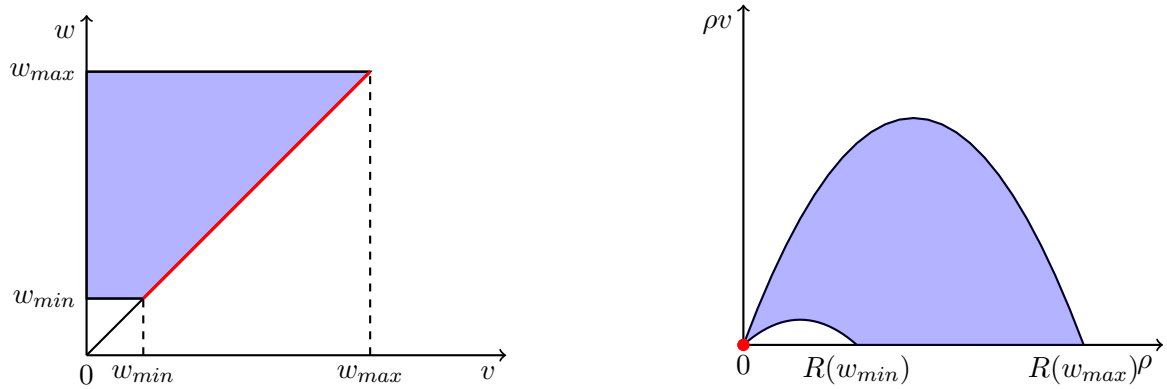

Figure 5. Invariant domain Ω (10) in the (v, w)-coordinates (left) and the $(\rho, \rho v)$-coordinates (rigtht). Vacuum states are highlighted in red.

We recall that, for Temple class systems, general well-posedness results [21–23] (for initial data with possibly unbounded total variation) hold under the assumption of strict hyperbolicity. For system (6), we observe that

$$\lambda_1(0, w) = \mathcal{V}(0, w) = w = \lambda_2(0, w),$$

showing that strict hyperbolicity is lost at vacuum. While existence of solutions can still be proved for data which are BV in the Riemann invariants [24,25], uniqueness does not hold if vacuum is involved. Let us consider for example a Riemann-like initial datum of the form

$$(\rho^0, w^0)(x) = \begin{cases} (\rho_L, w_L) & \text{if } x < 0, \\ (0, w_R) & \text{if } x > 0, \end{cases} \tag{11}$$

with $\rho_L > 0$ and $w_L \geq w_R > 0$ such that $\mathcal{V}(\rho_L, w_L) < \mathcal{V}(0, \rho_R)$. One solution consists of a first family rarefaction wave followed by a contact discontinuity

$$(\rho_1, w_1)(t, x) = \begin{cases} (\rho_L, w_L) & \text{if } x < \lambda_1(\rho_L, w_L)t, \\ \lambda_1^{-1}(x/t) & \text{if } \lambda_1(\rho_L, w_L)t \leq x < \lambda_1(\rho_M, w_L)t, \\ (\rho_M, w_L) & \text{if } \lambda_1(\rho_M, w_L)t \leq x < w_R t, \\ (0, w_R) & \text{if } x \geq w_R t, \end{cases}$$

where (ρ_M, w_L) is an intermediate state satisfying $\mathcal{V}(\rho_M, w_L) = w_R$. A second one can be constructed as a first family rarefaction wave connecting the left state directly to the vacuum, followed by a vacuum wave (not visible, since it has no physical meaning), as proposed in [24]:

$$(\rho_2, w_2)(t, x) = \begin{cases} (\rho_L, w_L) & \text{if } x < \lambda_1(\rho_L, w_L)t, \\ \lambda_1^{-1}(x/t) & \text{if } \lambda_1(\rho_L, w_L)t \leq x < \lambda_1(0, w_L)t, \\ (0, w_L) & \text{if } x \geq \lambda_1(0, w_L)t. \end{cases}$$

The two solutions are illustrated in Figure 6. Notice that they are both weak entropy solutions in the sense of Lax [26].

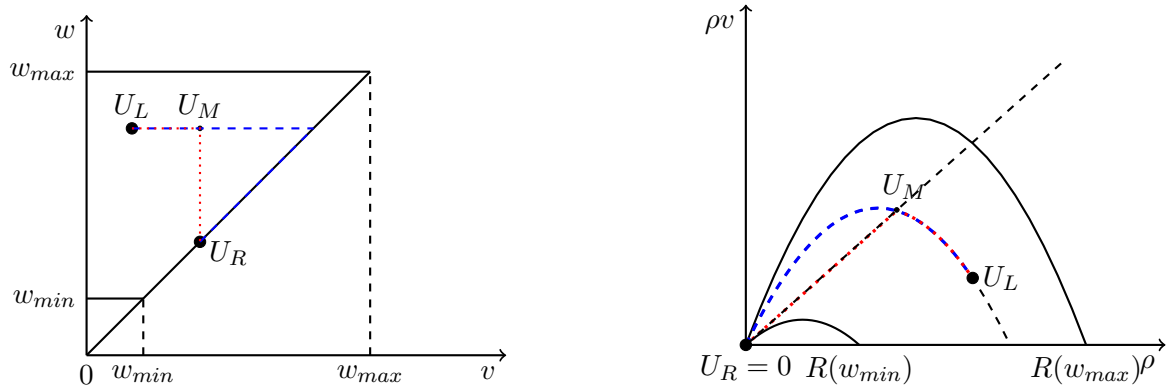

Figure 6. Two entropy admissible solutions to the Riemann problem (6)-(11) in two different coordinate systems: (ρ_1, w_1) is depicted in dotter red, (ρ_2, w_2) in dashed blue.

The intrinsic instability at vacuum of second order models, which poses issues for their analytical and numerical treatment, has been addressed introducing the so called *phase-transition models* [27,28]. The idea is to couple second order models describing the congested dynamics with the first order LWR equation (3) accounting for free flow conditions, by introducing a transition dynamics between free and congested flows. In particular, free flow and congested phases can be distinguished in model (6) by taking speed laws of the form

$$v = \min\{V_{\max}, \mathcal{V}(\rho, w)\},$$

for some $0 < V_{\max} < w_{min}$ as in [29,30], or

$$v = \begin{cases} v_e(\rho) & \text{if } 0 \le \rho \le \rho_f, \\ \mathcal{V}(\rho, w) & \text{if } \rho_f < \rho \le R_{\max}, \end{cases}$$

for some $\rho_f \in]0, R_{\max}[$ such that $\mathcal{V}(\rho_f, w) = v_e(\rho_f)$ for all $w \in [w_{min}, w_{max}]$ to ensure continuity, as proposed by [31]. Such models turn out to be well posed for general BV data [32].

2.1. *Numerical approximations*

The most widely used numerical scheme for traffic flow macroscopic simulations is the finite volume Godunov scheme [33] in its Cell Transmission Model (CTM) version [34], where the fluxes across interfaces are given by the minimum of the sending capacity of the upstream cell and the receiving capacity at the downstream one.

Given a space step Δx and a time step Δt satisfying the CFL condition

$$\max_{(\rho,w)\in\Omega} \{|\lambda_1(\rho, w)|, |\lambda_2(\rho, w)|\}\Delta t \le \Delta x,$$

let $x_{j+1/2} = j\Delta x$, $j \in \mathbb{Z}$, be the cells interfaces, and $t^n = n\Delta t$, $n \in \mathbb{N}$, the time mesh.
Denoting by $U = (\rho, y)^T = (\rho, \rho w)^T$ the vector of the conservative variables (where we set $y = \rho w$), we construct a finite volume approximate solution of (6) of the form $U^{\Delta x} = (\rho^{\Delta x}, y^{\Delta x})^T$ with $\rho^{\Delta x}(t, x) = \rho_j^n$ and $y^{\Delta x}(t, x) = y_j^n$ for $(t, x) \in C_j^n = [t^n, t^{n+1}[\times [x_{j-1/2}, x_{j+1/2}[$. To this end, we approximate the initial data with piece-wise constant functions

$$\rho_j^0 = \frac{1}{\Delta x}\int_{x_{j-1/2}}^{x_{j+1/2}} \rho^0(x)\,dx, \quad y_j^0 = \frac{1}{\Delta x}\int_{x_{j-1/2}}^{x_{j+1/2}} y^0(x)\,dx, \qquad \forall j \in \mathbb{Z},$$

and we iterate in time according to the conservation formulas

$$\rho_j^{n+1} = \rho_j^n - \frac{\Delta t}{\Delta x}\left(F_{j+1/2}^{\rho,n} - F_{j-1/2}^{\rho,n}\right), \tag{12a}$$

$$y_j^{n+1} = y_j^n - \frac{\Delta t}{\Delta x}\left(F_{j+1/2}^{y,n} - F_{j-1/2}^{y,n}\right), \tag{12b}$$

where $F_{j+1/2}^{\rho,n}$ and $F_{j+1/2}^{y,n}$ are the the flow respectively of ρ and y at $x = x_{j+1/2}$ in the time interval $[t^n, t^{n+1}[$. Let us remark that, since the variable w is advected with ρv, we get

$$F_{j+1/2}^{y,n} = w_j^n F_{j+1/2}^{\rho,n}. \tag{13}$$

in (12b). To compute $F_{j+1/2}^{\rho,n}$, we define the corresponding demand and supply functions [35,36] as

$$D_j = D(\rho_j, w_j) = \begin{cases} Q(\rho_j, w_j) & \text{if } \rho_j \le \rho_{cr}(w_j), \\ Q_{\max}(w_j) & \text{if } \rho_j > \rho_{cr}(w_j), \end{cases}$$

$$S_{j+1} = S(\rho_{j+1}, w_{j+1}; w_j) = \begin{cases} Q_{\max}(w_j) & \text{if } \rho_{j+1/2} \le \rho_{cr}(w_j), \\ Q(\rho_{j+1/2}, w_j) & \text{if } \rho_{j+1/2} > \rho_{cr}(w_j), \end{cases}$$

where $\rho_{j+1/2}$ is the density of the intermediate state in the solution of the Riemann problem corresponding to U_j and U_{j+1}:

$$\begin{array}{lll} \rho_{j+1/2} \quad \text{such that} \quad \mathcal{V}(\rho_{j+1/2}, w_j) = \mathcal{V}(\rho_{j+1}, w_{j+1}) & & \text{if } \mathcal{V}(\rho_{j+1}, w_{j+1}) \le w_j; \\ 0 & & \text{if } \mathcal{V}(\rho_{j+1}, w_{j+1}) > w_j. \end{array}$$

We can thus set

$$F_{j+1/2}^{\rho,n} = \min\left\{D(\rho_j^n, w_j^n), S(\rho_{j+1}^n, w_{j+1}^n; w_j^n)\right\} \tag{14}$$

in (12), (13). See [31] for a physical interpretation of demand and supply functions, and the role of the intermediate state.

Remark 2.1. Taking $w_j^0 = \bar{w}$ constant, the scheme (12)-(14) boils down to the standard CTM approximation of the LWR model (3):

$$\rho_j^{n+1} = \rho_j^n - \frac{\Delta t}{\Delta x}\left(F_{j+1/2}^{n} - F_{j-1/2}^{n}\right),$$

with

$$F_{j+1/2}^{n} = \min\left\{D(\rho_j^n), S(\rho_{j+1}^n)\right\}$$

and

$$D(\rho_j) = \begin{cases} Q(\rho_j, \bar{w}) & \text{if } \rho_j \le \rho_{cr}(\bar{w}), \\ Q_{\max}(\bar{w}) & \text{if } \rho_j > \rho_{cr}(\bar{w}), \end{cases} \qquad S(\rho_{j+1}) = \begin{cases} Q_{\max}(\bar{w}) & \text{if } \rho_{j+1} \le \rho_{cr}(\bar{w}), \\ Q(\rho_{j+1}, \bar{w}) & \text{if } \rho_{j+1} > \rho_{cr}(\bar{w}). \end{cases}$$

3. Macroscopic models for heterogeneous traffic flows

The macroscopic models presented above are based on the assumption that vehicles' characteristics are homogeneous, and traffic flow is mainly impacted by drivers' behaviour (modeled by the Lagrangian marker w). In real situations, the vehicles present on a road can differ a lot by technical characteristics, like size and speed. Think for example of cars and trucks: beside their size, trucks generally run at lower speed with respect to cars (because of the imposed speed limits, but also due to their lower acceleration). Also, the foreseen deployment of autonomous vehicles on public roads is expected to impact the overall traffic conditions due to their different dynamics. For these reasons, real traffic flows can be better described accounting for possible vehicle heterogeneities.

3.1. *Multi-class models*

When the number of vehicles in each class is of the same order, it is still meaningful to represent each class dynamics at a macroscopic level. Denoting by ρ^c, $c = 1, \dots, N$, the density of the c-th class, the mass conservation law holding for each class leads to the $N \times N$ system of equations

$$\partial_t \rho^c + \partial_x(\rho^c v_c) = 0, \qquad c = 1, \dots, N, \tag{15}$$

coupled by the speed functions v_c, which model each class behaviour depending on the different class densities:

$$v_c = v_c(\rho^1, \dots, \rho^N). \tag{16}$$

Different coupling laws (16) are proposed in the literature, depending on the targeted application: interaction dynamics can vary greatly if we consider mixed flows of cars and trucks obeying lane discipline [37–40], or a disordered flow of cars and two-wheelers without any lane rule [41–43]. Indeed, in the latter case, we may observe creeping behaviour of cycles, stemming form the fact that jam densities (for which $v_c = 0$) are different for cars and cycles, the latter still being able to advance when cars are stopped.

Taking $v_c(\rho_1, \dots, \rho^N) = V^c_{\max}\Psi(r)$ as in [39], where $r = \sum_{c=1}^N \rho^c / R^c_{\max}$ is the total (normalized) traffic density, $V^1_{\max} > \dots > V^N_{\max}$ are the classes' maximal speeds and $\Psi : [0,1] \to [0,1]$ is a decreasing function satisfying $\Psi(0) = 1$ and $\Psi(1) = 0$, the multi-class model (15) is defined on the simplex

$$\mathcal{S} := \left\{ (\rho_1, \dots, \rho^N) \in \mathbb{R}^N : \sum_{i=1}^N \rho_i \le 1, \rho_i \ge 0 \text{ for } i = 1, \dots, N \right\}.$$

System

$$\partial_t \rho^c + \partial_x(V^c_{\max}\, \rho^c \Psi(r)) = 0, \qquad c = 1, \dots, N,$$

is hyperbolic, but lacks of strict hyperbolicity at *umbilic points* on the boundaries of $\mathcal{S}$ (with $\rho_i = 0$ for some $i = 1, \dots, N$), hindering its analytical study. Nevertheless, numerical simulations show that the model can display observed behaviour, like overtaking of slower vehicles by faster ones, see Figure 7. In

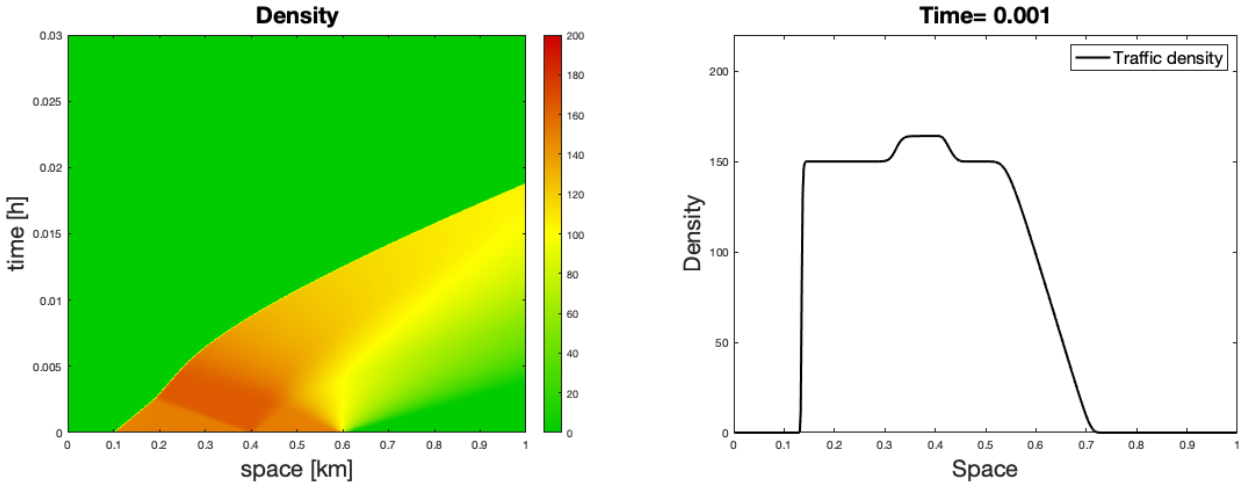

Figure 7. Solution of (15) with $V^1_{\max} = 140$ km/h, $V^2_{\max} = 100$ km/h and $R^1_{\max} = R^2_{\max} = 200$ veh/km, corresponding to the initial data $\rho^0_1(x) = 0.75 R_{\max}\chi([0.1, 0.4])$ and $\rho^0_2(x) = 0.75 R_{\max}\chi(]0.4, 0.6])$ This situation describes queue dissolution at a traffic light located at $x = 0.6$ and turning to green at $t = 0$, with a group of more aggressive divers initially located behind slower ones, which causes a congestion formation behind the downstream group, where density reaches higher levels than the initial ones. Left: (t, x) plot of the total density $(\rho^1 + \rho^2)$. Right: total density profile at $t = 0.001$ h. We can observe the upstream shock and the downstream rarefaction, separated by an higher density region. The global behaviour is similar to the one obtained using the ARZ model in Figure 4.

this case, instead of using the multi-class equivalent of Godunov flux, as proposed by [42] (and which

displays oscillations due to unbounded total variation), we propose the following extension of the upwind scheme first introduced by [44,45]

$$\rho_j^{c,n+1} = \rho_{1,j}^{c,n} - \frac{\Delta t}{\Delta x}\left(F_{j+1/2}^{c,n} - F_{j-1/2}^{c,n}\right), \qquad c = 1, \dots, N,$$

with

$$F_{j+1/2}^{c,n} = V_{\max}^c \, \rho_{1,j}^{c,n} \, \Psi(r_{j+1}^n), \qquad c = 1, \dots, N.$$

Remark 3.1. The invariance of $\mathcal{S}$ for $N > 2$ and general existence results for $N \geq 2$ are currently open problems.

3.2. *Multi-scale models*

If a class consists of a small number of vehicles, compared to the bulk traffic, it can be modeled microscopically by a system of Ordinary Differential Equations (ODEs) describing each vehicle's trajectory and coupled with the partial differential equations (PDEs) giving the macroscopic traffic evolution. Besides other approaches [46,47], the capacity reduction due to the presence of a slow vehicle can be accounted by a moving flux inequality constraints, as proposed by [48–50]. More precisely, equations (6) are coupled with the following laws

$$\dot{\xi}(t) = \min\{V(t), v(t, \xi(t)+)\}, \tag{17a}$$

$$\lim_{x \to \xi(t)\pm} \Big(\rho(t,x)(v(t,x) - \dot{\xi}(t))\Big) \leq F_\alpha(\dot{\xi}(t)), \tag{17b}$$

where $V(t) \in \mathbf{W}^{\mathbf{1,1}}_{\mathbf{loc}}(\mathbb{R}^+;\mathbb{R}^+)$ is the desired speed of the slow vehicle, and $x = \xi(t)$ its position at time $t > 0$. The upper bound in (17b) accounts for the road capacity reduction due to the presence of the vehicle, which acts as a moving bottleneck: $\alpha \in]0,1[$ is the reduction rate, and F_α is the corresponding maximal flow attainable at the vehicle's position:

$$F_\alpha(\dot{\xi}(t)) := \rho_\alpha^2 \mathcal{V}(\rho_\alpha, w_\alpha),$$

where $w_\alpha \in]w_{min}, w_{max}[$ satisfies $R(w_\alpha) = \alpha R(w_{max})$ and $\rho_\alpha \in]0, \alpha R(w_{max})[$ is the point of maximum of the relative flow function $\psi(\rho) = \rho\left(\mathcal{V}(\rho, w_\alpha) - \dot{\xi}(t)\right)$, i.e.

$$\mathcal{V}(\rho_\alpha, w_\alpha) + \rho_\alpha \mathcal{V}_\rho(\rho_\alpha, w_\alpha) = \dot{\xi}(t).$$

Classical solutions of (6) remain admissible provided that the relative flux at $x = \xi(t)$ does not exceed the upper bound $F_\alpha(\dot{\xi}(t))$. Otherwise, the enforcement of constraint (17b) causes the formation of a *undercompressive shock*, that is a non-classical jump discontinuity which satisfies the Rankine-Hugoniot conditions, thus guaranteeing conservation, but violates Lax entropy conditions. More precisely, let $U_L = (\rho_L, w_L)$, $U_R = (\rho_R, w_R) \in \Omega$ and consider the Cauchy problem for (6)-(17) corresponding to the initial data

$$(\rho, w)(0, x) = \begin{cases} (\rho_L, w_L) & \text{if } x < 0, \\ (\rho_R, w_R) & \text{if } x > 0, \end{cases} \tag{18a}$$

$$\xi(0) = 0, \tag{18b}$$

and to the constant bottleneck speed $\dot{\xi}(t) = \bar{V}$ for all $t > 0$. Let $I(w_L)$ be the set

$$I(w_L) = \{\rho \in [0, R(w_{max})] \colon \rho \mathcal{V}(\rho, w_L) = F_\alpha(\bar{V}) + \rho \bar{V}\}.$$

Since the map $\rho \mapsto \rho\left(\mathcal{V}(\rho, w_L)) - \bar{V}\right)$ is strictly concave due to (7b), the set $I(w_L)$ contains at most two elements. If $I(w_L) \neq \emptyset$, let $\hat{\rho} = \hat{\rho}(w_L)$ and $\check{\rho} = \check{\rho}(w_L)$ be the points defined by

$$\hat{\rho}(w_L) = \max I(w_L), \qquad \check{\rho}(w_L) = \min I(w_L).$$

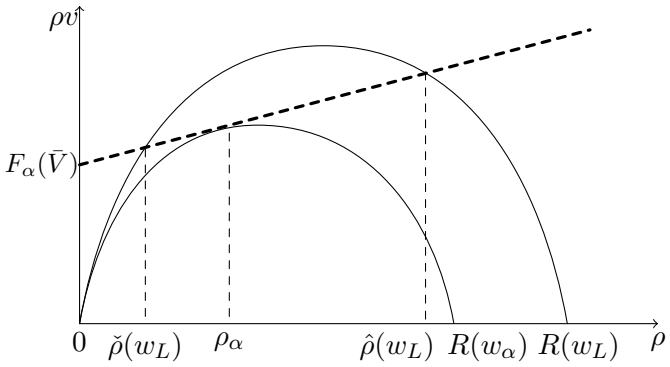

Figure 8. The definition of $\check\rho(w_L)$ and $\hat\rho(w_L)$.

These are respectively the points with maximal and minimal density of the Lax curve of the first family passing through (ρ_L, w_L) which satisfy the condition (17b) on the flux, see Figure 8.

Let now $\mathcal{R}_{GSOM}$ be the standard Riemann solver for (6), see e.g. [51] for a detailed description, and let

$$\bar\rho(U_L, U_R)(\cdot) \quad \text{and} \quad \bar w(U_L, U_R)(\cdot)$$

be respectively the ρ and w components of $\mathcal{R}_{GSOM}(U_L, U_R)(\cdot)$, and let

$$f_1(\mathcal{R}_{GSOM}(U_L, U_R)(\cdot)) := \bar\rho(U_L, U_R)(\cdot)\, \mathcal{V}\left(\bar\rho(U_L, U_R)(\cdot), \bar w(U_L, U_R)(\cdot)\right)$$

be the first component of the flux function of the GSOM system.

An admissible Riemann solver $\mathcal{R}^\alpha_{GSOM}$ for the constrained GSOM system (6)-(17) can be constructed as follows.

1. If $f_1(\mathcal{R}_{GSOM}(U_L, U_R)(\bar V)) > F_\alpha(\bar V) + \bar V\, \bar\rho(U_L, U_R)(\bar V)$, then

$$\mathcal{R}^\alpha_{GSOM}(U_L, U_R)(x/t) = \begin{cases} \mathcal{R}_{GSOM}((\rho_L, w_L), (\hat\rho, w_L))(x/t) & \text{if } x < y(t), \\ \mathcal{R}_{GSOM}((\check\rho, w_L), (\rho_R, w_R))(x/t) & \text{if } x > y(t), \end{cases}$$

and $y(t) = \bar V\, t$, see Figure 9.

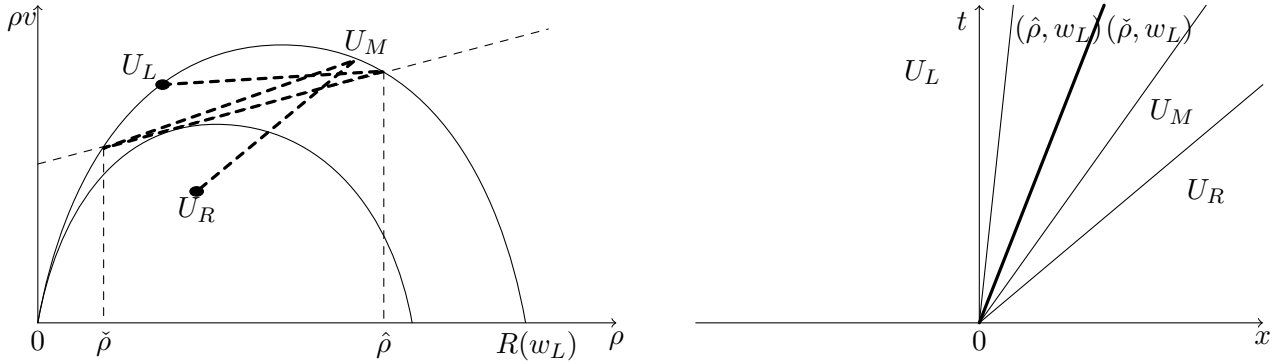

Figure 9. The constrained Riemann problem (6)-(17), case 1. In this case $\xi(t) = \xi(0) + \bar V\, t$, while the solution (ρ, w) is composed by two classical shocks of the first family separated by an undercompressive shock between $(\hat\rho, w_L)$ and $(\check\rho, w_L)$, all followed by a contact discontinuity. The unconstrained solution would have consisted of a classical shock from U_L to $U_M = (\rho_M, w_L)$ with $\mathcal{V}(\rho_M, w_L) = \mathcal{V}(\rho_R, w_R)$, followed by a contact discontinuity from U_M to U_R.

2. If $f_1(\mathcal{R}_{GSOM}(U_L, U_R)(\bar V)) \le F_\alpha(\bar V) + \bar V\, \bar\rho(U_L, U_R)(\bar V)$ then

$$\mathcal{R}^\alpha_{GSOM}(U_L, U_R)(x/t) = \mathcal{R}_{GSOM}(U_L, U_R)(x/t)$$

and $y(t) = \min\left\{\bar V, \mathcal{V}\left(\bar\rho(U_L, U_R)(\bar V), \bar w(U_L, U_R)(\bar V)\right)\right\} t$.

Remark that the solution $\mathcal{R}^{\alpha}_{GSOM}$ is conservative for both the traffic density and the momentum. An alternative solution conserving only the number of vehicles is proposed in [52]. Moreover, in case 1., the solution given by $\mathcal{R}^{\alpha}_{GSOM}$ does not satisfy the Lax entropy condition at the jump discontinuity between the left state $(\hat{\rho}, w_L)$ and the right state $(\check{\rho}, w_L)$, because $\check{\rho} < \hat{\rho}$ and thus $\lambda_1(\check{\rho}, w_L) > \lambda_1(\hat{\rho}, w_L)$. Therefore, $(\hat{\rho}, w_L)$ and $(\check{\rho}, w_L)$ are connected by a *non-classical shock*.

In the case $w_{min} = w_{max}$, the constrained GSOM system (6)-(17) boils down to the constrained LWR model described in [49], see Figure 11. In this case, existence and stability of solutions satisfying a suitable entropy condition has been proved in [50,53]. Also, the above construction can be extended to several, possibly interacting, moving bottlenecks, see [54].

Non-classical shocks arising at the bottleneck positions cannot be captured by classical (entropic) finite volume schemes, and they require a specific treatment, see e.g. [55–57]. The conservative reconstruction strategy proposed in [52,58] consists of using the classical Godunov scheme (12)-(14) away from bottleneck locations. Let C^n_m the cell where the moving bottleneck is located at time t^n, i.e. $\xi_n \simeq \xi(t^n) \in [x_{m-1/2}, x_{m+1/2}[$, and we set $U^n_j = (\rho^n_j, w^n_j)$. If

$$f_1(\mathcal{R}_{GSOM}(U^n_{m-1}, U^n_{m+1})(\bar{V})) > F_\alpha(\bar{V}) + \bar{V}\,\bar{\rho}(U^n_{m-1}, U^n_{m+1})(\bar{V}),$$

a non-classical shock is expected to arise in cell C^n_m, and the left and right numerical fluxes $F^{\rho,n}_{m\pm1/2}$ and $F^{y,n}_{m\pm1/2}$ are to be recomputed as follows. We replace the (constant) cell values ρ^n_m and y^n_m by the functions

$$\begin{aligned}\rho^n_{\text{rec}} &= \hat{\rho}(w^n_{m-1})\mathbf{1}_{[x_{m-1/2},\bar{x}^\rho_m[} + \check{\rho}(w^n_{m-1})\mathbf{1}_{[\bar{x}^\rho_m,x_{m+1/2}[},\\ y^n_{\text{rec}} &= \hat{y}(w^n_{m-1})\mathbf{1}_{[x_{m-1/2},\bar{x}^y_m[} + \check{y}(w^n_{m-1})\mathbf{1}_{[\bar{x}^y_m,x_{m+1/2}[},\end{aligned}$$

where

$$\bar{x}^\rho_m = x_{m-1/2} + h\,d^{\rho,n}_m \quad \text{and} \quad \bar{x}^y_m = x_{m-1/2} + h\,d^{y,n}_m$$

with

$$d^{\rho,n}_m = \frac{\rho^n_m - \check{\rho}(w^n_{m-1})}{\hat{\rho}(w^n_{m-1}) - \check{\rho}(w^n_{m-1})} \in [0,1] \qquad \text{and} \qquad d^{y,n}_m = \frac{y^n_m - \check{y}(w^n_{m-1})}{\hat{y}(w^n_{m-1}) - \check{y}(w^n_{m-1})} \in [0,1], \tag{19}$$

to guarantee conservation in both the ρ and y components, see Figure 10. Above, we have set $\hat{y}(w^n_{m-1}) = \hat{\rho}(w^n_{m-1})\,w^n_{m-1}$ and $\check{y}(w^n_{m-1}) = \check{\rho}(w^n_{m-1})\,w^n_{m-1}$. Since the non-classical shock travels with speed $\bar{V} > 0$,

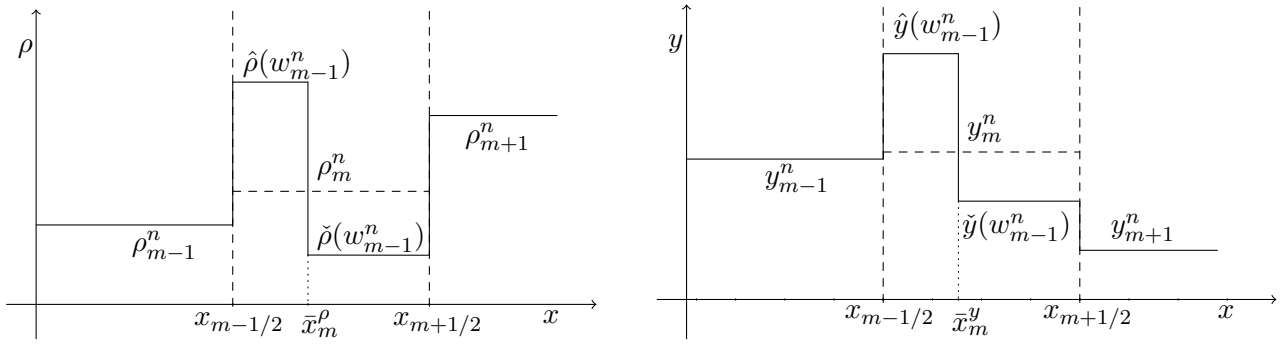

Figure 10. Non-classical shock numerical reconstruction.

we denote $\Delta t^\rho_{m+1/2}$ and $\Delta t^y_{m+1/2}$ respectively the time needed by the ρ and the y component of the discontinuity to reach the interface $x_{m+1/2}$:

$$\Delta t^\rho_{m+1/2} = \Delta x\,\frac{1 - d^{\rho,n}_m}{\bar{V}}\,, \qquad \Delta t^y_{m+1/2} = \Delta x\,\frac{1 - d^{y,n}_m}{\bar{V}}\,.$$

Therefore, we replace the classical Godunov flux $F^{\rho,n}_{m+1/2}$ by

$$\widetilde{F}^{\rho,n}_{m+1/2} = \frac{1}{\Delta t}\Big[\min(\Delta t^{\rho}_{m+1/2}, \Delta t)\check{\rho}(w^n_{m-1})\mathcal{V}(\check{\rho}(w^n_{m-1}), w^n_{m-1}) + \max(\Delta t - \Delta t^{\rho}_{m+1/2}, 0)\hat{\rho}(w^n_{m-1})\mathcal{V}(\hat{\rho}(w^n_{m-1}), w^n_{m-1})\Big],$$

and $F^{y,n}_{m+1/2}$ by $\widetilde{F}^{y,n}_{m+1/2} = w^n_{m-1}\,\widetilde{F}^{\rho,n}_{m+1/2}$. Also, we replace $F^{\rho,n}_{m-1/2}$ by

$$\widetilde{F}^{\rho,n}_{m-1/2} = \min\left\{D(\rho^n_{m-1}, w^n_{m-1}), S(\hat{\rho}(w^n_{m-1}), w^n_{m-1}; w^n_{m-1})\right\}$$

and $F^{y,n}_{m-1/2}$ by $\widetilde{F}^{y,n}_{m-1/2} = w^n_{m-1}\,\widetilde{F}^{\rho,n}_{m-1/2}$.

Figure 11 displays de solution computed with the above scheme in the case $w_{min} = w_{max}$ (and hence w constant), where we have applied the reconstruction technique also to the classical shock. Observe that both jump discontinuities are sharply captured.

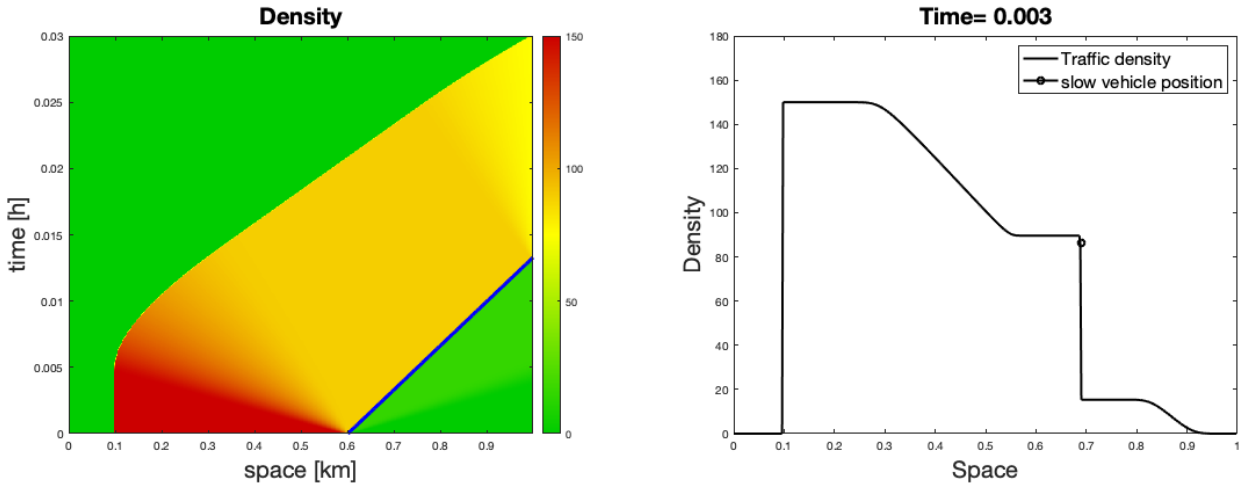

Figure 11. Solution of (6)-(17), with $\mathcal{V}(\rho, w) = V_{\max}\left(1 - \frac{\rho}{R_{\max}}\right)$, where $V_{\max} = 100$ km/h and $R_{\max} = 150$ veh/km, corresponding to the initial datum $\rho^0(x) = R_{\max}\chi([0.1, 0.6])$ and describing queue dissolution at a traffic light located at $x = 0.6$ and turning to green at $t = 0$. The presence of a slower vehicle at $\xi(0) = 0.6$, running at $V(t) = 30$ km/h and reducing by half the capacity of the road ($\alpha = 0.5$), hinders the traffic flow upstream of it (compare with Figure 2). Left: (t, x) density plot and slow vehicle trajectory (in blue). Right: density profile at $t = 0.003$ h. We can observe the nonclassical shock at the slow vehicle position.

4. Conclusions and perspectives

Macroscopic models can be used for estimation and prediction, but also as a basis to design control actions intended to optimize traffic flow on road networks, by improving throughput, reducing travel times and fuel consumption. Traditional optimization measures include variable message signs (such as traffic adaptive speed limits and dynamic routing), traffic-light control at intersections and ramp metering, or selective measures for specific vehicle classes (such as overtaking or circulation bans for trucks). We refer the reader to [59,60] for an overview of these approaches.

More recently, the expected deployment of Connected and Automated Vehicles (CAVs) has captured the attention of researchers as it offers the possibility to use CAVs as endogenous controls acting as moving bottlenecks, thus reducing traffic speed upstream. The benefits induced by CAV control have already been demonstrated experimentally [61,62] and make the object of model-based theoretical studies [63–66] as well as machine learning investigations [67,68]. In particular, the multi-scale models presented in Section 3.2 can be used to quantify the gain that can be obtained by controlling the desired speed of small fleets of CAVs in mixed traffic flows. As an example, we illustrate in Figure 12 the result of total fuel

consumption minimization algorithms using a centralized control of a small fleet of CAVs [69], supporting the perspective of regulating traffic flow by means of a small number of controlled vehicles.

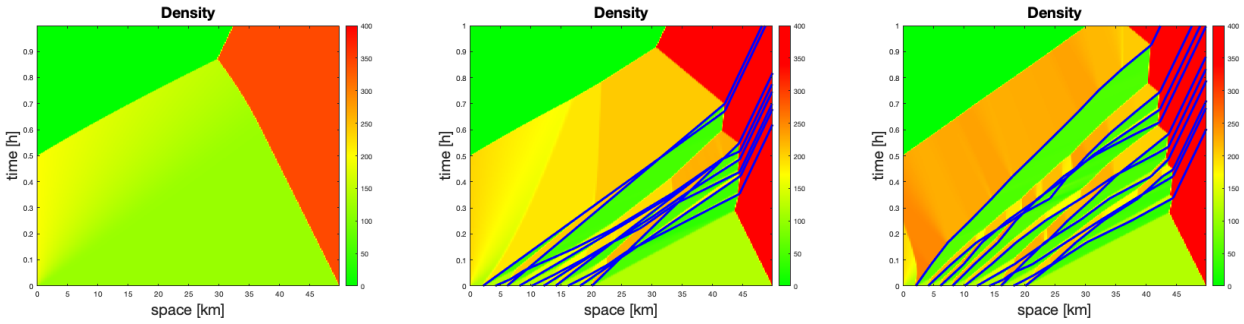

Figure 12. Traffic flow optimization on a 50 km road stretch by centralized control of a fleet of 10 CAVs initially equally distributed in the interval $[2, 20]$. Here we have used model (6)-(17), with $\mathcal{V}(\rho, w) = V_{\max}\left(1 - \frac{\rho}{R_{\max}}\right)$, where $V_{\max} = 140$ km/h and $R_{\max} = 400$ veh/km, and inflow and outflow boundary conditions are given by $f_{in}(t) = 1400\chi([0, 0.5])$ veh/h and $f_{out}(t) = 700\chi([0, 1])$ veh/h respectively. The cost function to be minimized is the Total Fuel Consumption (TFC) as described in [64]. We can observe on the left the non controlled situation, in the middle the solution corresponding to the optimal constant speed values on 1 hour time interval, on the right the solution given a Model Predictive Control algorithm corresponding to 15 min optimization updated every 5 min. The corresponding gain in TFC is 5.6% and 3.2% respectively, but we can also observe a consistent reduction of the congestion (in red).

References

1. M. J. Lighthill and G. B. Whitham, On kinematic waves. II. A theory of traffic flow on long crowded roads, *Proc. Roy. Soc. London Ser. A*, vol. 229, pp. 317–345, 1955.
2. P. I. Richards, Shock waves on the highway, *Operations Res.*, vol. 4, pp. 42–51, 1956.
3. B. Haut and G. Bastin, A second order model of road junctions in fluid models of traffic networks, *Netw. Heterog. Media*, vol. 2, no. 2, pp. 227–253, 2007.
4. B. Seibold, M. R. Flynn, A. R. Kasimov, and R. R. Rosales, Constructing set-valued fundamental diagrams from jamiton solutions in second order traffic models, *Netw. Heterog. Media*, vol. 8, no. 3, pp. 745–772, 2013.
5. H. Payne, Models of freeway traffic and control., in *Mathematical Models of Public Systems* (G. Bekey, ed.), vol. 1, pp. 51–61, 1971.
6. G. B. Whitham, *Linear and nonlinear waves*. Pure and Applied Mathematics, Wiley-Interscience [John Wiley & Sons], New York-London-Sydney, 1974.
7. C. F. Daganzo, Requiem for second-order fluid approximations of traffic flow, *Transportation Research Part B: Methodological*, vol. 29, no. 4, pp. 277–286, 1995.
8. A. Aw and M. Rascle, Resurrection of "second order" models of traffic flow, *SIAM J. Appl. Math.*, vol. 60, no. 3, pp. 916–938, 2000.
9. H. M. Zhang, A non-equilibrium traffic model devoid of gas-like behavior, *Transportation Res. Part B*, vol. 36, no. 3, pp. 275–290, 2002.
10. A. Klar and R. Wegener, A hierarchy of models for multilane vehicular traffic. I. Modeling, *SIAM J. Appl. Math.*, vol. 59, no. 3, pp. 983–1001, 1999.
11. R. M. Colombo and A. Corli, Well posedness for multilane traffic models, *Ann. Univ. Ferrara Sez. VII Sci. Mat.*, vol. 52, no. 2, pp. 291–301, 2006.
12. H. Holden and N. H. Risebro, Models for dense multilane vehicular traffic, *SIAM J. Math. Anal.*, vol. 51, no. 5, pp. 3694–3713, 2019.
13. M. Garavello, K. Han, and B. Piccoli, *Models for vehicular traffic on networks*, vol. 9 of *AIMS Series on Applied Mathematics*. American Institute of Mathematical Sciences (AIMS), Springfield, MO, 2016.

14. S. Blandin and P. Goatin, Well-posedness of a conservation law with non-local flux arising in traffic flow modeling, *Numer. Math.*, vol. 132, no. 2, pp. 217–241, 2016.
15. J. Friedrich, O. Kolb, and S. Göttlich, A Godunov type scheme for a class of LWR traffic flow models with non-local flux, *Netw. Heterog. Media*, vol. 13, no. 4, pp. 531–547, 2018.
16. J.-P. Lebacque, S. Mammar, and H. H. Salem, Generic second order traffic flow modelling, in *Transportation and Traffic Theory 2007*, 2007.
17. S. Fan, M. Herty, and B. Seibold, Comparative model accuracy of a data-fitted generalized Aw-Rascle-Zhang model, *Netw. Heterog. Media*, vol. 9, no. 2, pp. 239–268, 2014.
18. F. A. Chiarello, J. Friedrich, P. Goatin, and S. Göttlich, Micro-macro limit of a nonlocal generalized Aw-Rascle type model, *SIAM J. Appl. Math.*, vol. 80, no. 4, pp. 1841–1861, 2020.
19. A. Bressan, *Hyperbolic systems of conservation laws*, vol. 20 of *Oxford Lecture Series in Mathematics and its Applications*. Oxford: Oxford University Press, 2000. The one-dimensional Cauchy problem.
20. B. Temple, Systems of conservation laws with invariant submanifolds, *Trans. Amer. Math. Soc.*, vol. 280, no. 2, pp. 781–795, 1983.
21. P. Baiti and A. Bressan, The semigroup generated by a Temple class system with large data, *Differential Integral Equations*, vol. 10, no. 3, pp. 401–418, 1997.
22. S. Bianchini, Stability of L^∞ solutions for hyperbolic systems with coinciding shocks and rarefactions, *SIAM J. Math. Anal.*, vol. 33, no. 4, pp. 959–981, 2001.
23. A. Bressan and P. Goatin, Stability of L^∞ solutions of Temple class systems, *Differential Integral Equations*, vol. 13, no. 10-12, pp. 1503–1528, 2000.
24. B. Andreianov, C. Donadello, and M. D. Rosini, A second-order model for vehicular traffics with local point constraints on the flow, *Math. Models Methods Appl. Sci.*, vol. 26, no. 4, pp. 751–802, 2016.
25. M. Godvik and H. Hanche-Olsen, Existence of solutions for the Aw-Rascle traffic flow model with vacuum, *J. Hyperbolic Differ. Equ.*, vol. 5, no. 1, pp. 45–63, 2008.
26. P. D. Lax, Hyperbolic systems of conservation laws. II, *Comm. Pure Appl. Math.*, vol. 10, pp. 537–566, 1957.
27. R. M. Colombo, Hyperbolic phase transitions in traffic flow, *SIAM J. Appl. Math.*, vol. 63, no. 2, pp. 708–721, 2002.
28. P. Goatin, The Aw-Rascle vehicular traffic flow model with phase transitions, *Math. Comput. Modelling*, vol. 44, no. 3-4, pp. 287–303, 2006.
29. S. Blandin, D. Work, P. Goatin, B. Piccoli, and A. Bayen, A general phase transition model for vehicular traffic, *SIAM J. Appl. Math.*, vol. 71, no. 1, pp. 107–127, 2011.
30. R. M. Colombo, F. Marcellini, and M. Rascle, A 2-phase traffic model based on a speed bound, *SIAM J. Appl. Math.*, vol. 70, no. 7, pp. 2652–2666, 2010.
31. S. Fan, Y. Sun, B. Piccoli, B. Seibold, and D. B. Work, A collapsed generalized Aw-Rascle-Zhang model and its model accuracy, *arXiv preprint arXiv:1702.03624*, 2017.
32. R. M. Colombo, P. Goatin, and F. S. Priuli, Global well posedness of traffic flow models with phase transitions, *Nonlinear Anal.*, vol. 66, no. 11, pp. 2413–2426, 2007.
33. S. K. Godunov, A difference method for numerical calculation of discontinuous solutions of the equations of hydrodynamics, *Mat. Sb. (N.S.)*, vol. 47 (89), pp. 271–306, 1959.
34. C. F. Daganzo, The cell transmission model: A dynamic representation of highway traffic consistent with the hydrodynamic theory, *Transportation Research Part B: Methodological*, vol. 28, no. 4, pp. 269–287, 1994.
35. J. Lebacque, The Godunov scheme and what it means for first order traffic flow models, in *Proceedings of the 13th International Symposium on Transportation and Traffic Theory, Lyon, France, July*, vol. 2426, 1996.
36. J.-P. Lebacque, H. Haj-Salem, and S. Mammar, Second order traffic flow modeling: supply-demand analysis of the inhomogeneous Riemann problem and of boundary conditions, *Proceedings of the 10th Euro Working Group on Transportation (EWGT)*, vol. 3, no. 3, 2005.

37. G. Wong and S. Wong, A multi-class traffic flow model–an extension of LWR model with heterogeneous drivers, *Transportation Research Part A: Policy and Practice*, vol. 36, no. 9, pp. 827–841, 2002.
38. H. M. Zhang and W. L. Jin, Kinematic wave traffic flow model for mixed traffic, *Transportation Research Record*, vol. 1802, no. 1, pp. 197–204, 2002.
39. S. Benzoni-Gavage and R. M. Colombo, An n-populations model for traffic flow, *European J. Appl. Math.*, vol. 14, no. 5, pp. 587–612, 2003.
40. S. Chanut and C. Buisson, Macroscopic model and its numerical solution for two-flow mixed traffic with different speeds and lengths, *Transportation research record*, vol. 1852, no. 1, pp. 209–219, 2003.
41. R. Nair, H. S. Mahmassani, and E. Miller-Hooks, A porous flow approach to modeling heterogeneous traffic in disordered systems, *Procedia - Social and Behavioral Sciences*, vol. 17, pp. 611–627, 2011. Papers selected for the 19th International Symposium on Transportation and Traffic Theory.
42. S. Fan and D. B. Work, A heterogeneous multiclass traffic flow model with creeping, *SIAM J. Appl. Math.*, vol. 75, no. 2, pp. 813–835, 2015.
43. S. Gashaw, P. Goatin, and J. Härri, Modeling and analysis of mixed flow of cars and powered two wheelers, *Transportation Research Part C: Emerging Technologies*, vol. 89, pp. 148–167, 2018.
44. M. Hilliges and W. Weidlich, A phenomenological model for dynamic traffic flow in networks, *Transportation Research Part B: Methodological*, vol. 29, no. 6, pp. 407–431, 1995.
45. R. Bürger, A. García, K. H. Karlsen, and J. D. Towers, A family of numerical schemes for kinematic flows with discontinuous flux, *J. Engrg. Math.*, vol. 60, no. 3-4, pp. 387–425, 2008.
46. C. Lattanzio, A. Maurizi, and B. Piccoli, Moving bottlenecks in car traffic flow: a PDE-ODE coupled model, *SIAM J. Math. Anal.*, vol. 43, no. 1, pp. 50–67, 2011.
47. R. Borsche, R. M. Colombo, and M. Garavello, Mixed systems: ODEs - balance laws, *J. Differential Equations*, vol. 252, no. 3, pp. 2311–2338, 2012.
48. J. Lebacque, J. Lesort, and F. Giorgi, Introducing buses into first-order macroscopic traffic flow models, *Transportation Research Record*, vol. 1644, no. 1, pp. 70–79, 1998.
49. M. L. Delle Monache and P. Goatin, Scalar conservation laws with moving constraints arising in traffic flow modeling: an existence result, *J. Differential Equations*, vol. 257, no. 11, pp. 4015–4029, 2014.
50. M. Garavello, P. Goatin, T. Liard, and B. Piccoli, A multiscale model for traffic regulation via autonomous vehicles, *J. Differential Equations*, vol. 269, no. 7, pp. 6088–6124, 2020.
51. S. Fan, *Data-fitted generic second order macroscopic traffic flow models*. PhD thesis, Temple University, 2013.
52. S. Villa, P. Goatin, and C. Chalons, Moving bottlenecks for the Aw-Rascle-Zhang traffic flow model, *Discrete Contin. Dyn. Syst. Ser. B*, vol. 22, no. 10, pp. 3921–3952, 2017.
53. T. Liard and B. Piccoli, Well-posedness for scalar conservation laws with moving flux constraints, *SIAM J. Appl. Math.*, vol. 79, no. 2, pp. 641–667, 2019.
54. P. Goatin, C. Daini, M. L. Delle Monache, and A. Ferrara, Interacting moving bottlenecks in traffic flow, *Netw. Heterog. Media*, to appear.
55. C. F. Daganzo and J. A. Laval, On the numerical treatment of moving bottlenecks, *Transportation Research Part B: Methodological*, vol. 39, no. 1, pp. 31–46, 2005.
56. M. L. Delle Monache and P. Goatin, A numerical scheme for moving bottlenecks in traffic flow, *Bull. Braz. Math. Soc. (N.S.)*, vol. 47, no. 2, pp. 605–617, 2016. Joint work with C. Chalons.
57. M. Čičić, I. Mikolášek, and K. H. Johansson, Front tracking transition system model with controlled moving bottlenecks and probabilistic traffic breakdowns, *IFAC-PapersOnLine*, vol. 53, no. 2, pp. 14990–14996, 2020. 21st IFAC World Congress.
58. C. Chalons, M. L. Delle Monache, and P. Goatin, A conservative scheme for non-classical solutions to a strongly coupled PDE-ODE problem, *Interfaces Free Bound.*, vol. 19, no. 4, pp. 553–570, 2017.
59. M. Treiber and A. Kesting, *Traffic Flow Dynamics*. Berlin Heidelberg: Springer-Verlag, 2013.
60. A. Ferrara, S. Sacone, and S. Siri, *Freeway Traffic Modelling and Control*. Berlin Heidelberg: Springer,

2018.

61. R. E. Stern, S. Cui, M. L. Delle Monache, R. Bhadani, M. Bunting, M. Churchill, N. Hamilton, R. Haulcy, H. Pohlmann, F. Wu, B. Piccoli, B. Seibold, J. Sprinkle, and D. B. Work, Dissipation of stop-and-go waves via control of autonomous vehicles: Field experiments, *Transportation Research Part C: Emerging Technologies*, vol. 89, pp. 205–221, 2018.
62. R. E. Stern, Y. Chen, M. Churchill, F. Wu, M. L. Delle Monache, B. Piccoli, B. Seibold, J. Sprinkle, and D. B. Work, Quantifying air quality benefits resulting from few autonomous vehicles stabilizing traffic, *Transportation Research Part D: Transport and Environment*, vol. 67, pp. 351–365, 2019.
63. M. Čičić and K. H. Johansson, Traffic regulation via individually controlled automated vehicles: a cell transmission model approach, in *2018 21st International Conference on Intelligent Transportation Systems (ITSC)*, pp. 766–771, 2018.
64. G. Piacentini, P. Goatin, and A. Ferrara, Traffic control via moving bottleneck of coordinated vehicles, *IFAC-PapersOnLine*, vol. 51, no. 9, pp. 13–18, 2018.
65. M. Čičić and K. H. Johansson, Stop-and-go wave dissipation using accumulated controlled moving bottlenecks in multi-class CTM framework, in *2019 IEEE 58th Conference on Decision and Control (CDC)*, pp. 3146–3151, 2019.
66. G. Piacentini, P. Goatin, and A. Ferrara, Traffic control via platoons of intelligent vehicles for saving fuel consumption in freeway systems, *IEEE Control Syst. Lett.*, vol. 5, no. 2, pp. 593–598, 2021.
67. E. Vinitsky, K. Parvate, A. Kreidieh, C. Wu, and A. Bayen, Lagrangian control through Deep-RL: Applications to bottleneck decongestion, in *2018 21st International Conference on Intelligent Transportation Systems (ITSC)*, pp. 759–765, 2018.
68. A. R. Kreidieh, C. Wu, and A. M. Bayen, Dissipating stop-and-go waves in closed and open networks via deep reinforcement learning, in *2018 21st International Conference on Intelligent Transportation Systems (ITSC)*, pp. 1475–1480, 2018.
69. C. Daini, P. Goatin, M. L. D. Monache, and A. Ferrara, Centralized traffic control via small fleets of connected and automated vehicles, in *2022 European Control Conference (ECC)*, pp. 371–376, 2022.